

Weak universality induced by $Q = \pm 2e$ charges at the deconfinement transition of a $(2+1)$ -d $U(1)$ lattice gauge theory

Indrajit Sau,¹ Arnab Sen,¹ and Debasish Banerjee^{2,3}

¹*School of Physical Sciences, Indian Association for the Cultivation of Science, Kolkata 700032, India*

²*Theory Division, Saha Institute of Nuclear Physics, 1/AF Bidhan Nagar, Kolkata 700064, India*

³*Homi Bhabha National Institute, Training School Complex, Anushaktinagar, Mumbai 400094, India*
(Dated: September 30, 2022)

Matter-free lattice gauge theories (LGTs) provide an ideal setting to understand confinement to deconfinement transitions at finite temperatures, which is typically due to the spontaneous breakdown (at large temperatures) of the centre symmetry associated with the gauge group. Close to the transition, the relevant degrees of freedom (Polyakov loop) transform under these centre symmetries, and the effective theory only depends on the Polyakov loop and its fluctuations. As shown first by Svetitsky and Yaffe, and subsequently verified numerically, for the $U(1)$ LGT in $(2+1)$ -d the transition is in the 2-d XY universality class, while for the Z_2 LGT, it is in the 2-d Ising universality class. We extend this classic scenario by adding higher charged matter fields, and show that the notion of universality is generalized such that the critical exponents γ, ν can change continuously as a coupling is varied, while their ratio is fixed to the 2-d Ising value. While such weak universality is well-known for spin models, we demonstrate this for LGTs for the first time. Using an efficient cluster algorithm, we show that the finite temperature phase transition of the $U(1)$ quantum link LGT in the spin $S = \frac{1}{2}$ representation is in the 2-d XY universality class, as expected. On the addition of $Q = \pm 2e$ charges distributed thermally, we demonstrate the occurrence of weak universality.

Introduction.— Phases of matter at extreme physical conditions of temperature, pressure, and density often challenge our conventional notions and stimulate extensive research, both experimentally and theoretically. Of particular relevance are the physics of the early universe, and the interior of neutron stars. Both scenarios are expected to have a microscopic description through quantum chromodynamics (QCD), a field theory of quarks and gluons [1–4]. As a quantum field theory (QFT), QCD is a strongly interacting theory which confines colour-charge carrying quarks and gluons into colour singlet bound states, through the confinement phenomenon rendering conventional perturbation techniques unsuitable.

Lattice gauge theories (LGT) are non-perturbative formulation of QFTs, where Markov chain Monte Carlo methods are used to compute expectation values of physical observables, and supply the most reliable insights about the strong interaction physics [5]. The possibility of a phase transition out of the confined phase at finite temperatures was explored first using the computationally simpler case of matter-free pure gauge theories. It is universally accepted that pure $SU(3)$ gauge theory has a first order deconfinement phase transition [6, 7], while the $SU(2)$ gauge theory has a second order phase transition [8, 9]. For QCD with physical quark masses, there is only a crossover from the hadronic phase to the deconfined quark gluon plasma phase [10, 11].

The finite temperature phase transition in pure gauge theories can be described using an effective field theory (EFT). Svetitsky and Yaffe (SY) [12] used the insight that the confinement to deconfinement transition in a pure gauge theory is due to the spontaneous breakdown of the global centre symmetry of the gauge group to

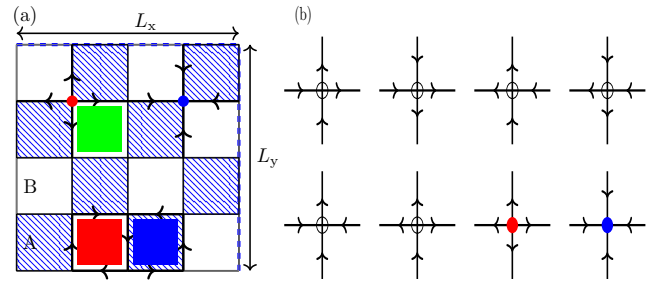


Figure 1. (a) Sketch of the lattice, the dashed and clear plaquettes denote the A and B sublattice respectively. $Q = \pm 2e$ charges are shown as red and blue circles, respectively. Plaquettes can be non-flippable (shaded in green), especially when it has a charge $\pm 2e$ at a corner, or flippable in the clockwise (red) or anti-clockwise (blue) sense. (b) The different Gauss law realizations which contribute with equal weight, the first six have $Q = 0$, while the last two have $Q = \pm 2e$ at the vertex.

show the relevant degrees of freedom in the EFT are the Polyakov loop (order parameter), and its fluctuations. Integrating out all other degrees of freedom in the original gauge theory in $(d+1)$ -dimensions, they argued that the EFT corresponds to a d -dimensional scalar field theory or spin system. The confinement in the original gauge theory ensures that the effective couplings in the spin system are all short ranged. Using universality, they argued that if the effective spin model has a second order transition, then the original gauge theory should also have it. This SY scenario has been verified in different numerical simulations [13–18], and is widely regarded as a success of universality.

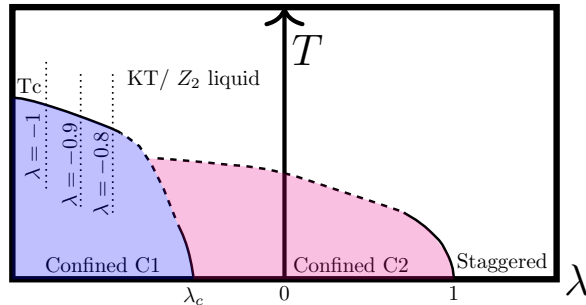


Figure 2. The $T - \lambda$ phase diagram: at $T = 0$ there are two confined phases (C1 and C2) separated by a weak first order phase transition. Beyond the Rokhsar-Kivelson point, $\lambda = 1$, the staggered phase is encountered. At high T , there is a pure $U(1)$ liquid, or a Z_2 liquid where $Q = \pm 2$ charges exist. In this paper, we study the finite temperature phase diagram. The dashed lines indicate a possible behaviour of the phase boundaries.

In this Letter, we report an extension of the SY approach of understanding the finite temperature phase transition of a (2+1)-d $U(1)$ lattice gauge theory in the presence of higher charges $\pm 2e$ (where e denotes the fundamental unit of charge, which we set to 1 henceforth). As we will demonstrate using a specific example of a quantum link model (QLM), the presence of the even charges keeps intact only a global Z_2 subgroup of the full $U(1)$ centre symmetry. Consequently, the SY prediction of a Berezinskii-Kosterlitz-Thouless (BKT) for the deconfinement transition of the pure $U(1)$ LGT gets modified. Instead, a weak universality phenomenon arises [19], characterized by large values of critical exponents like γ, ν, β , while others like η, δ defined directly at the critical point, as well as the ratios of the critical exponents are fixed to the 2-d Z_2 Ising model. Weak universality has been observed in a variety of systems [20–28], however; we demonstrate this at the finite-temperature deconfinement transition of a LGT for the first time. We perform extensive finite size scaling (FSS) studies on lattices upto $(512a)^2$ (a denotes the lattice spacing) with very small Trotter steps $\epsilon/J \sim 0.05$ (J denotes a microscopic coupling) to demonstrate the BKT as well as the weak universality scenario at the deconfinement transition in the absence and presence of the ± 2 charges, respectively.

Model, Simulations, and Phase Diagram.— The quantum link gauge theories we consider use quantum spin $S = \frac{1}{2}$ as degrees of freedom on the bonds $(x, \hat{\mu})$ between the sites of a square lattice. The electric flux operator, $E_{x, \hat{\mu}} = S_{x, \hat{\mu}}^3$, takes two values $\pm \frac{1}{2}$ while the gauge fields are the raising (lowering) operators of electric flux: $U_{x, \hat{\mu}}^{(\dagger)} = S_{x, \hat{\mu}}^{+(-)}$. The Hamiltonian operator is the sum of elementary plaquette terms

$$H = -J \sum_{\square} \left[(U_{\square} + U_{\square}^{\dagger}) - \lambda (U_{\square} + U_{\square}^{\dagger})^2 \right] \quad (1)$$

where $U_{\square} = U_{x, \hat{\mu}} U_{x+\hat{\mu}, \hat{\nu}} U_{x+\hat{\nu}, \hat{\mu}}^{\dagger} U_{x, \hat{\nu}}^{\dagger}$. We set the lattice spacing of the square lattice (a) as well as J to 1 henceforth. Figure 1 (a) shows the set-up of the lattice. The electric fluxes are shown as directed arrows. We note that $U_{\square}(U_{\square}^{\dagger})$ reverses the orientation of the electric flux around the plaquette (clockwise to anticlockwise and vice-versa), while all non-flippable plaquettes are annihilated. The λ term is akin to a potential energy, counting the total number of flippable plaquettes (both clockwise and anticlockwise). The local $U(1)$ symmetry is generated by the Gauss Law operator $G_x = \sum_{\hat{\mu}} (E_{x, \hat{\mu}} - E_{x-\hat{\mu}, \hat{\mu}})$, and thus divides the Fock space into (exponentially) large number of superselection sectors. The physical states in the vacuum sector satisfy $G_x |\psi\rangle = 0$ (six allowed states for each vertex of the square lattice) for all sites x . Additionally, the presence of $Q = \pm 2$, extends the Gauss Law to also include $G_x |\phi\rangle = \pm 2 |\phi\rangle$. Imposing periodic boundary conditions, only states which have zero total charge are allowed. Figure 1 (b) shows all the allowed configurations (six with $Q_x = 0$, one each with $Q_x = 2$ and $Q_x = -2$) in our model, all allowed with equal weights. A detailed discussion about the symmetries is given in the Supp. Mat. At finite temperature $T = 1/\beta$, the equilibrium properties can be obtained from the partition function Z :

$$Z = \text{Tr} \left[e^{-\beta H} \prod_x \{6\delta(G_x) + \delta(G_x - 2) + \delta(G_x + 2)\} \frac{1}{8} \right], \quad (2)$$

along with the charge neutrality constraint, $\sum_x Q_x = 0$.

While the charges $Q = \pm 2$ do not have a kinetic energy term in the Hamiltonian, they are generated thermally, and move around the lattice due to thermal fluctuations. The $Q = \pm 2$ charges can be regarded as an example of *annealed disorder* [29] where these “impurities” are in thermal equilibrium with the rest of the system according to Equation (2). As one would naively expect from a confining theory, at $T = 0$, the charges are high energy states, and thus do not appear. However, close to the deconfinement phase transition (when $T \sim \lambda J \sim M$, where M is the rest mass of the charges), the charges are thermally generated, and therefore affect the critical properties of the system as we demonstrate later. In the Supp. Mat., we show how the presence of $Q = \pm 2$ charges gives rise to an effective Z_2 Gauss’ Law for the theory.

In Figure 2, we sketch a finite temperature phase diagram of the model with and without the charges. The phase transition in λ (at $T = 0$) revealed two distinct crystalline confined phases (C1 and C2) separated by a weak first order phase transition at $\lambda_c \sim -0.36$ [30, 31]. The phases can be understood via a two-component magnetization (measured respectively on sublattice A and B , see Figure 1 (a)). In phase C1, both sublattices order (spontaneously breaking the lattice translation and charge conjugation), while for phase C2 only one of the sublattices order (breaking lattice translations). On rais-

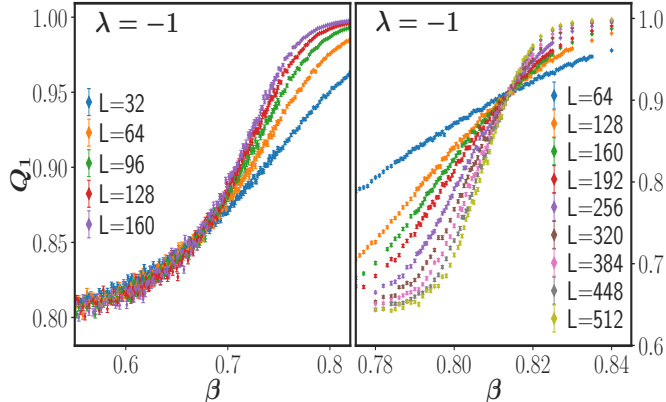


Figure 3. The Binder cumulant, Q_1 , for the $U(1)$ QLM without (left) and with (right) the charges $Q = \pm 2$. The former displays a 2-d XY scenario (critical high-T and gapped low-T phase), while the latter exhibits a 2-d Ising scenario (gapped high-T and low-T) phases as one would expect from the SY analysis. We demonstrate weak universality for the latter case.

ing the temperature, one expects the symmetry breakings to disappear accompanied by a spontaneous breaking of the global $U(1)^2$ symmetry, and SY analysis suggests a BKT phase transition. With the charges $Q = \pm 2$ in the ensemble, the quantum phase transition remains unchanged, while the thermal transition is modified. Due to the charges, the $U(1)^2$ centre symmetry is reduced to the Z_2^2 global center symmetry that breaks as the temperature is raised, leading one to naively expect a second order phase transition with 2-d Z_2 critical exponents. However, the thermal transition now displays properties associated with weak universality.

We study the model using a cluster quantum Monte Carlo (QMC) algorithm, which can efficiently update the (Kramers-Wannier) dualized version of the model [32] on a lattice with L (L_T) number of points in the spatial (temporal) direction. The algorithm builds clusters on the height variables $h^{A,B}$, placed at the centre of either the A or the B sublattices (see Figure 1), which are then flipped. A comparison of the QMC results, both in the absence and presence of $Q = \pm 2$ charges, with exact diagonalization (ED) results on small lattices is shown in Supp. Mat. The sublattice magnetizations are defined using the height variables as $M_X = \frac{1}{L_T} \sum_{\tilde{x}} \eta_{\tilde{x}}^X h_{\tilde{x}}^X$, where $X = A, B$ and \tilde{x} denote the dual sites (centres of the plaquettes of the original space-time lattice). The phase factors $\eta_{\tilde{x}}^X$ are necessary to capture the ordering of the height variables corresponding to the flippability of the plaquettes. In the Supp. Mat., we show that (M_A, M_B) serve as order parameters for the deconfinement transition. For finite size scaling (FSS) studies, we use total

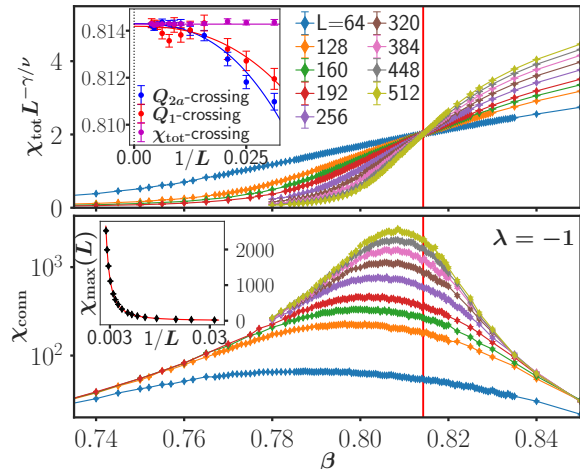


Figure 4. (Top) The critical temperature β_c of the theory with charges is estimated by the crossing of χ_{tot} for different L . (Inset) Estimates of β_c using Q_1 and Q_{2a} yield consistent results. (Bottom) Plot of χ_{conn} vs β for various L shows a peak, whose scaling with L (inset) is used to extract γ/ν . The vertical line denotes β_c .

and connected susceptibilities:

$$\chi_{\text{tot}} = \frac{1}{V} \langle M^2 \rangle, \quad \chi_{\text{conn}} = \frac{\beta}{V} \sum_X (\langle M_X^2 \rangle - \langle |M_X| \rangle^2), \quad (3)$$

where $M^2 = \sum_{X=A,B} (M_X^2)$, $V = L^2$, and $\beta = \epsilon L_T$. Three different Binder cumulants were also used to estimate the critical exponents:

$$Q_1 = \frac{1}{2} \sum_X \frac{\langle |M_X| \rangle^2}{\langle M_X^2 \rangle}; \quad Q_{2a} = 2 - \frac{\langle M^4 \rangle}{\langle M^2 \rangle^2}; \quad (4)$$

$$Q_{2b} = \frac{3}{2} - \frac{1}{4} \sum_X \frac{\langle M_X^4 \rangle}{\langle M_X^2 \rangle^2}.$$

Finite temperature transition and FSS.— The FSS hypothesis for the order parameter predicts that the Binder cumulants are universal at the critical point [33–35]. We use this feature to show that the theory with and without the charges have different thermal behaviour. In the left panel of Figure 3 (the pure $U(1)$ theory), the Binder Q_1 curves for different lattice sizes L collapse on each other at high-T, while they differ in the low-T phase. This is the expected behaviour for an XY-universality, where a critical phase goes into a massive phase through the BKT transition. The right panel shows Q_1 for the $U(1)$ theory with charges $Q = \pm 2$ for different L , which cross each other at $\beta_c \approx 0.815$, the probable location of a second order phase transition. We will postpone a detailed study of the BKT phase transition in a future publication, since it establishes the conventional wisdom, and concentrate here solely on the second order transition.

L_T	β_c	η	$\nu(Q_1)$	$\nu(Q_{2a})$	$\nu(Q_{2b})$
$\lambda = -1.0$					
24	0.814279(14)	0.2472(9)	1.35(2)	1.38(1)	1.38(2)
16	0.813783(15)	0.2479(9)	1.32(4)	1.34(2)	1.34(4)
8	0.811129(14)	0.2489(8)	1.33(3)	1.31(2)	1.34(3)
4	0.801059(12)	0.2509(8)	1.29(1)	1.31(1)	1.29(2)
2	0.767685(10)	0.2497(7)	1.19(1)	1.20(1)	1.20(1)
$\lambda = -0.9$					
24	0.885292(17)	0.2550 (18)	1.45(3)	1.47(4)	1.45(3)
$\lambda = -0.8$					
24	0.968196(26)	0.2511 (10)	1.64(9)	1.68(4)	1.64(8)

Table I. Estimates of β_c , η , and ν in the thermodynamic limit for different values of L_T and λ .

We extract the critical temperature $T_c = 1/\beta_c$ from crossing points of the curves of three different observables ($\chi_{\text{tot}}L^{-\gamma/\nu}$, Q_1 , and Q_{2a}). Figure 4 (top panel) shows $\chi_{\text{tot}}L^{-\gamma/\nu}$ vs β for $L = 64, \dots, 512$ and $L_T = 24$. In this analysis, we fixed $\gamma/\nu = 7/4$, the value for 2-d, Z_2 universality class. We will derive this independently later, and fitting for the ratio γ/ν only increases the uncertainties without any gain. Moreover, we need very precise estimates of β_c to compute ν . Using a second order polynomial interpolation to extract the crossing points of lattices ($L, 2L$), we observe a surprisingly flat behaviour for estimates of $\beta_c(L)$ from χ_{tot} as a function of $1/L$, as shown in the inset. Estimates of β_c were also extracted from the crossing points of Q_1 and Q_{2a} curves. As shown in the inset, those estimates have larger finite size corrections, but yield the same β_c for $L > 100$. Therefore, we quote the value of $\beta_c(L \rightarrow \infty, L_T = 24)$ by fitting a constant to the β_c estimates from χ_{tot} , and report it in Table I for different L_T values and three different $\lambda = -1.0, -0.9, -0.8$ values.

We turn to the estimate of the critical exponents. The scaling of the peak of χ_{conn} , $\chi_{\text{conn,max}}(L) = bL^{\gamma/\nu} = bL^{2-\eta}$ can be reliably used to extract η (and thus also γ/ν). This quantity is shown (in a semi log scale) in Figure 4 (bottom panel) vs β , with the vertical line indicating β_c in the thermodynamic limit. The inset shows a power law fit to the $1/L$ dependence of χ_{conn} , from which η is extracted, and reported for all our lattices and λ values in Table I. The systematic and the statistical errors are very well controlled in our data and analysis procedure, and yields estimates of η for different L_T and λ , consistent with the 2d Z_2 universality class. The largest deviation is only at the 3σ level for $L_T = 24$ and $\lambda = -1$, while most values are consistent with $\eta = \frac{1}{4}$ within 1σ . Moreover, this is also consistent with weak universality, where deviation from the critical exponent ratios is not observed.

Weak universality.– The next step to substantiate our claim involves the accurate computation of ν in-

dependently, for which we use all three Binder ratios. We employ the well-known result [35, 36] that for a dimensionless phenomenological coupling $R(\beta, L)$, the slope at β_c directly yields the exponent ν , $\left. \frac{\partial R(L)}{\partial \beta} \right|_{\beta_c} = aL^{1/\nu}(1 + bL^{-\omega})$. For large lattices (or for large ω), plotting the derivative (at β_c) vs L in a log-log scale enables us to compute $1/\nu$ from the slope. The crucial requirement here is the very precise estimate of β_c , which we have already described. Performing this analysis using all three Binder ratios gives us consistent estimates of ν . The particular analysis for Q_{2a} for $L_T = 24$ and three different $\lambda = -1.0, -0.9, -0.8$ is shown in Figure 5. To obtain the derivatives, we first fit the Binder ratios around β_c to second order polynomials, and then take the derivative analytically with respect to β . Note that since the Binder ratios are all $O(1)$ numbers, and have a smooth behaviour around β_c , the polynomial fit is free of any systematic errors. Statistical errors are computed using bootstrapping samples from the entire data set. While the data is sufficiently accurate to extract reliable estimates of ν , we are unable to estimate any reliable estimate of ω , the leading correction to the scaling exponent. However, it is clear from the figure that the slopes of the curve (horizontally and vertically displaced for better visibility) are significantly different from the 2d Z_2 universality class value of $\nu = 1$. Instead, we witness significantly large values of ν as extracted from the coupling Q_{2a} : 1.38(1) for $\lambda = -1.0$, 1.47(4) for $\lambda = -0.9$, and 1.68(4) for $\lambda = -0.8$. These values are collected in Table I, along with the corresponding estimates from the Q_1 and Q_{2b} . We note that all three estimates of ν at a fixed λ agree with each other, and increase monotonically with λ . In particular, the inset of Figure 5 displays this variation clearly. Not only are these values of ν anomalously large, but they also vary smoothly with the microscopic coupling. Both these features are hallmarks of weak universality.

An intriguing question is the reason for the occurrence of weak universality. According to the theory of renormalization group, a marginal operator [29, 37, 38] is needed to generate a line of fixed points with continuously varying critical exponents. While we cannot yet offer an explicit realization of such an operator, we note that it would likely depend on the $Q = \pm 2$ charges. In Supp. Mat., we show the behavior of $\langle Q^2 \rangle$ (normalized with the volume) as a function of β at $\lambda = -1, -0.9, -0.8$. A small yet non-zero ($\langle Q^2 \rangle \approx 0.03$ where $\langle Q^2 \rangle_{\text{max}} = 1$ as $T \rightarrow \infty$) critical density of charges in the vicinity of β_c suggests that charged operators play a non-trivial role in deciding the critical properties.

Conclusions and outlook.– In this article, we demonstrated that the presence of charges can completely alter the thermal phase transition in a pure gauge theory, using the example of a (2+1)-d $U(1)$ QLM, by plotting the Binder cumulant across the phase transition (Figure 3).

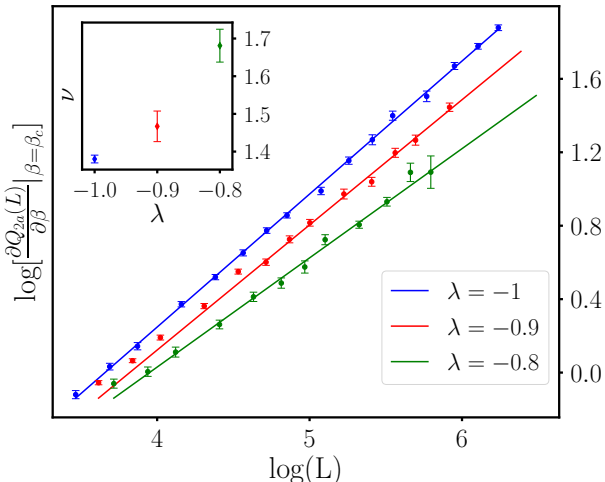


Figure 5. Extraction of ν from the slope of derivative of Q_{2a} at β_c . The three curves correspond to different λ which are vertically and horizontally displaced for better visibility. The inset shows the change of slope (and hence ν) with λ .

Using $\chi_{\text{tot}}(L)$, and the Binder ratios, we located β_c very accurately, and then used the scaling of $\chi_{\text{conn,max}}(L)$ to compute η , which is compatible with the 2-d Z_2 value, as expected from universality arguments. Finally, using three Binder ratios, we demonstrate that the individual exponents ν (and γ) have anomalously large values compared to the 2-d Z_2 value, and furthermore vary smoothly as a function of the microscopic coupling λ . These three pieces of evidence conclusively show that weak universality is relevant for this thermal transition instead of the usual universality scenario.

Our results open some very intriguing directions for further research. A close examination of the charge and the electric flux distribution at β_c could help to provide a better understanding of a possible marginal operator that leads to weak universality. It is also interesting to follow the thermal transition to more negative values of λ to explore whether it reaches the 2d Z_2 limit. Finally, exploring the phase diagram where three phases (C1, C2, and KT/ Z_2 liquid) meet is an exciting project for the future. The prospect that this model could be realized in quantum simulator set-ups in the recent future makes these results potentially interesting [39, 40]. Whether such weak universality also happens for other gauge theories is an open question to be explored by the community.

We would like to thank Shailesh Chandrasekharan and Uwe-Jens Wiese for useful discussions. We acknowledge the computational resources provided by IACS and SINP. D.B. acknowledges assistance from SERB Starting grant SRG/2021/000396-C from the DST (Govt. of India).

- [1] Frank Wilczek, “QCD in extreme conditions,” *9th CRM Summer School: Theoretical Physics at the End of the 20th Century*, , 567–636 (1999), [arXiv:hep-ph/0003183](#).
- [2] Owe Philipsen, “Constraining the phase diagram of QCD at finite temperature and density,” *PoS LATTICE2019*, 273 (2019), [arXiv:1912.04827 \[hep-lat\]](#).
- [3] Massimo D’Elia, “High-Temperature QCD: theory overview,” *Nucl. Phys. A* **982**, 99–105 (2019), [arXiv:1809.10660 \[hep-lat\]](#).
- [4] Sayantan Sharma, “Recent theoretical developments on QCD matter at finite temperature and density,” *Int. J. Mod. Phys. E* **30**, 2130003 (2021), [arXiv:2103.13641 \[hep-lat\]](#).
- [5] Andreas S. Kronfeld *et al.* (USQCD), “Lattice QCD and Particle Physics,” (2022), [arXiv:2207.07641 \[hep-lat\]](#).
- [6] Michael Creutz and K. J. M. Moriarty, “Numerical Studies of Wilson Loops in SU(3) Gauge Theory in Four-dimensions,” *Phys. Rev. D* **26**, 2166 (1982).
- [7] John B. Kogut, J. Polonyi, H. W. Wyld, J. Shigemitsu, and D. K. Sinclair, “Further Evidence for the First Order Nature of the Pure Gauge SU(3) Deconfinement Transition,” *Nucl. Phys. B* **251**, 311–332 (1985).
- [8] M. Creutz, “Monte Carlo Study of Quantized SU(2) Gauge Theory,” *Phys. Rev. D* **21**, 2308–2315 (1980).
- [9] R. V. Gavai, “The Deconfinement Transition in SU(2) Lattice Gauge Theories,” *Nucl. Phys. B* **215**, 458–469 (1983).
- [10] P. Hasenfratz, F. Karsch, and I. O. Stamatescu, “The SU(3) Deconfinement Phase Transition in the Presence of Quarks,” *Phys. Lett. B* **133**, 221–226 (1983).
- [11] Tanmoy Bhattacharya *et al.*, “QCD Phase Transition with Chiral Quarks and Physical Quark Masses,” *Phys. Rev. Lett.* **113**, 082001 (2014), [arXiv:1402.5175 \[hep-lat\]](#).
- [12] Benjamin Svetitsky and Laurence G. Yaffe, “Critical behavior at finite-temperature confinement transitions,” *Nuclear Physics B* **210**, 423–447 (1982).
- [13] M. Caselle and M. Hasenbusch, “Deconfinement transition and dimensional crossover in the 3-D gauge Ising model,” *Nucl. Phys. B* **470**, 435–453 (1996), [arXiv:hep-lat/9511015](#).
- [14] Claudio Bonati and Massimo D’Elia, “Phase diagram of the 4D U(1) model at finite temperature,” *Phys. Rev. D* **88**, 065025 (2013), [arXiv:1305.3564 \[hep-lat\]](#).
- [15] Richard Lau and Michael Teper, “The deconfining phase transition of SO(N) gauge theories in 2+1 dimensions,” *JHEP* **03**, 072 (2016), [arXiv:1510.07841 \[hep-lat\]](#).
- [16] Oleg Borisenko, Volodymyr Chelnokov, Francesca Cuteri, and Alessandro Papa, “Berezinskii-Kosterlitz-Thouless phase transitions in two-dimensional non-Abelian spin models,” *Phys. Rev. E* **94**, 012108 (2016), [arXiv:1512.05737 \[hep-lat\]](#).
- [17] Minati Biswal, Mridupawan Deka, Sanatan Digal, and P. S. Saumia, “Confinement-deconfinement transition in SU(2) Higgs theory,” *Phys. Rev. D* **96**, 014503 (2017), [arXiv:1610.08265 \[hep-lat\]](#).
- [18] Yoshinobu Kuramashi and Yusuke Yoshimura, “Three-dimensional finite temperature Z_2 gauge theory with tensor network scheme,” *JHEP* **08**, 023 (2019), [arXiv:1808.08025 \[hep-lat\]](#).
- [19] M. Suzuki, “New Universality of Critical Exponents,” *Progress of Theoretical Physics* **51**, 1992–1993 (1974).

- [20] R. J. Baxter, “Eight-Vertex Model in Lattice Statistics,” *Physical Review Letters* **26**, 832–833 (1971).
- [21] J. Ashkin and E. Teller, “Statistics of Two-Dimensional Lattices with Four Components,” *Physical Review* **64**, 178–184 (1943).
- [22] P. A. Pearce and D. Kim, “Continuously varying exponents in magnetic hard squares,” *Journal of Physics A Mathematical General* **20**, 6471–6485 (1987).
- [23] Fabien Alet, Jesper Lykke Jacobsen, Grégoire Misguich, Vincent Pasquier, Frédéric Mila, and Matthias Troyer, “Interacting Classical Dimers on the Square Lattice,” *Physical Review Letters* **94**, 235702 (2005), arXiv:cond-mat/0501241 [cond-mat.stat-mech].
- [24] A. Malakis, A. Nihat Berker, I. A. Hadjiagapiou, and N. G. Fytas, “Strong violation of critical phenomena universality: Wang-Landau study of the two-dimensional Blume-Capel model under bond randomness,” *Physical Review E* **79**, 011125 (2009), arXiv:0809.4241 [cond-mat.dis-nn].
- [25] S. L. A. de Queiroz, “Scaling behavior of a square-lattice Ising model with competing interactions in a uniform field,” *Physical Review E* **84**, 031132 (2011), arXiv:1107.6022 [cond-mat.stat-mech].
- [26] Songbo Jin, Arnab Sen, and Anders W. Sandvik, “Ashkin-Teller Criticality and Pseudo-First-Order Behavior in a Frustrated Ising Model on the Square Lattice,” *Physical Review Letters* **108**, 045702 (2012), arXiv:1110.5874 [cond-mat.stat-mech].
- [27] Songbo Jin, Arnab Sen, Wenan Guo, and Anders W. Sandvik, “Phase transitions in the frustrated Ising model on the square lattice,” *Phys. Rev. B* **87**, 144406 (2013).
- [28] Takafumi Suzuki, Kenji Harada, Haruhiko Matsuo, Synge Todo, and Naoki Kawashima, “Thermal phase transition of generalized Heisenberg models for SU(N) spins on square and honeycomb lattices,” *Physical Review B* **91**, 094414 (2015), arXiv:1505.06273 [cond-mat.stat-mech].
- [29] John Cardy, *Scaling and Renormalization in Statistical Physics*, Cambridge Lecture Notes in Physics (Cambridge University Press, 1996).
- [30] D. Banerjee, F. J. Jiang, P. Widmer, and U. J. Wiese, “The (2 + 1)-d U(1) quantum link model masquerading as deconfined criticality,” *J. Stat. Mech.* **1312**, P12010 (2013), arXiv:1303.6858 [cond-mat.str-el].
- [31] Ferdinand Tschirsich, Simone Montangero, and Marcello Dalmonte, “Phase diagram and conformal string excitations of square ice using gauge invariant matrix product states,” *SciPost Physics* **6**, 028 (2019), arXiv:1807.00826 [cond-mat.stat-mech].
- [32] Debasish Banerjee, “Recent progress on cluster and meron algorithms for strongly correlated systems,” *Indian J. Phys.* **95**, 1669–1680 (2021), arXiv:2101.03161 [hep-lat].
- [33] K. Binder, “Monte Carlo calculation of the surface tension for two- and three-dimensional lattice-gas models,” *Phys. Rev. A* **25**, 1699 (1982).
- [34] K. S. D. Beach, Ling Wang, and Anders W. Sandvik, “Data collapse in the critical region using finite-size scaling with subleading corrections,” (2005), 10.48550/ARXIV.COND-MAT/0505194.
- [35] Ling Wang, K. S. D. Beach, and Anders W. Sandvik, “High-precision finite-size scaling analysis of the quantum-critical point of $s = 1/2$ Heisenberg antiferromagnetic bilayers,” *Phys. Rev. B* **73**, 014431 (2006).
- [36] Martin Hasenbusch, “Finite size scaling study of lattice models in the three-dimensional Ising universality class,” *Phys. Rev. B* **82**, 174433 (2010), arXiv:1004.4486 [cond-mat.stat-mech].
- [37] Jorge V. José, Leo P. Kadanoff, Scott Kirkpatrick, and David R. Nelson, “Renormalization, vortices, and symmetry-breaking perturbations in the two-dimensional planar model,” *Phys. Rev. B* **16**, 1217–1241 (1977).
- [38] Gesualdo Delfino and Noel Lamsen, “Critical points of coupled vector-ising systems. exact results,” *Journal of Physics A: Mathematical and Theoretical* **52**, 35LT02 (2019).
- [39] D. Marcos, P. Widmer, E. Rico, M. Hafezi, P. Rabl, U. J. Wiese, and P. Zoller, “Two-dimensional Lattice Gauge Theories with Superconducting Quantum Circuits,” *Annals Phys.* **351**, 634–654 (2014), arXiv:1407.6066 [quant-ph].
- [40] Alessio Celi, Benoît Vermersch, Oscar Viyuela, Hannes Pichler, Mikhail D. Lukin, and Peter Zoller, “Emerging Two-Dimensional Gauge Theories in Rydberg Configurable Arrays,” *Phys. Rev. X* **10**, 021057 (2020), arXiv:1907.03311 [quant-ph].

Supplementary Material

Symmetries with and without static ± 2 charges

In this section, we discuss the various symmetries of the model with and without the ± 2 charges. Let us first discuss the case without the charges, where one has the usual lattice symmetries of translations by one lattice spacing, the various reflection and rotation symmetries which form the point group symmetries. The charge conjugation is a global internal Z_2 symmetry, which transforms as: $U \rightarrow U^\dagger, U^\dagger \rightarrow U, E \rightarrow -E$. Additionally, there is the global symmetry associated with the large gauge transformations, generated by the operator $W_i = \frac{1}{L_i} \sum_x E_{x,i}$ and classifies the physical states in winding sectors taking values in \mathbb{Z} for even L . Finally, the gauge symmetry, corresponding to the choice of the Gauss Law allows only the six allowed states with zero charge at a vertex.

We note that the QLM with spin $S = \frac{1}{2}$ has a different ground state phase diagram from the Wilsonian LGT. The latter uses quantum rotors as degrees of freedom, and thus the electric flux are quantized in integer units, whereas in our case the electric flux is always $\pm \frac{1}{2}$. The QLM ground state diagram has three distinct phases: two different confined phases (C1 and C2), and the staggered phase. For large negative λ , where phase C1 is stabilized, the ground state has the maximal number of flippable plaquettes (see Figure 6 (left)). This phase spontaneously breaks lattice translation symmetry by one lattice spacing, as well as charge conjugation symmetry. As λ is reduced, the J term governing the flips dominate, and the system goes into a new phase (C2) where one of the two sublattices (for example, the shaded one) is in a coherent superposition of clockwise and anticlockwise flippable plaquettes, often called a resonating valence bond (RVB) solid. C2 has an unbroken charge conjugation symmetry, but a still broken lattice translation symmetry. In terms of magnetization operators (introduced in the Main text), in the phase C1 both sublattices are ordered, while C2 has ordering of one of the two sublattices.

When the ± 2 charges are included in the thermal ensemble (by appropriately modifying the Gauss Law), several of the previous global symmetries do not remain good quantum numbers any more. Since the distribution of charges in the volume is governed thermally, lattice translation, rotation and reflections are not good symmetries. Charge conjugation is explicitly broken in the presence of charges. The total number of allowed states at a vertex is now 8, out of the 16 possible states in total. The other 8 states correspond to the presence of a ± 1 charge, and are realized in the quantum dimer model, but not in our model. With 8 vertex states allowed by the Gauss Law, this is an effective Z_2 gauge constraint on

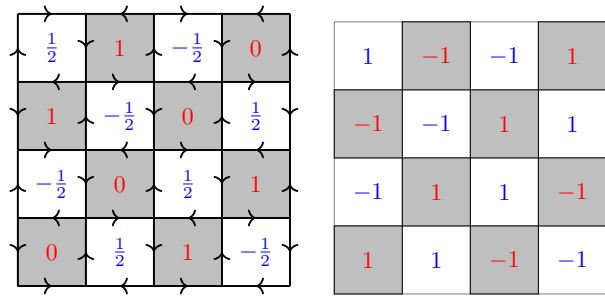


Figure 6. (Left): Reference configuration for a $L = 4$ lattice. Such a configuration has the maximum number of flippable plaquettes, which is signalled by large values of both M_A, M_B . Both the flux (on the links) and the height variables (in the dual lattices) are shown. (Right) The phase factors η_x^X for the A and B sublattices which need to be multiplied with the height variables h^X to obtain the magnetization.

the Hamiltonian in Equation (1). It can also be viewed as a quantum eight-vertex model. A more mathematical argument is provided below to make the effective Z_2 nature of the Gauss Law explicit. The winding numbers now take values in $\mathbb{Z}/2$ for even L .

Since the Gauss law for the pure gauge theory annihilates the physical states $|\psi\rangle$, it follows that the action of an arbitrary gauge transformation on the physical states keeps them unchanged:

$$\begin{aligned} V|\psi\rangle &= \prod_x \exp(i\theta_x G_x) |\psi\rangle \\ &= \prod_x \left[1 + i\theta_x G_x - \frac{\theta_x^2 G_x^2}{2} + \dots \right] |\psi\rangle = |\psi\rangle. \end{aligned} \quad (5)$$

The $U(1)$ nature of the gauge symmetry is because $\theta_x \in (0, 2\pi]$ is an angle. When we allow $Q_x = 0, \pm 2$ in our theory, then we have two classes of states, $|\Psi\rangle = \{|\psi\rangle, |\phi\rangle\}$, which satisfy, $G_x |\psi\rangle = 0$ and $G_x |\phi\rangle = \pm 2 |\phi\rangle$. Under the same gauge transformation as before, we now have

$$\begin{aligned} V|\Psi\rangle &= \prod_x \exp(i\theta_x G_x) |\Psi\rangle \\ &= \prod_x \left[1 + i\theta_x G_x - \frac{\theta_x^2 G_x^2}{2} + \dots \right] |\Psi\rangle \end{aligned} \quad (6)$$

For the states $|\psi\rangle$ it is clearly satisfied, but for the states $|\phi\rangle$, the states are only unchanged when $\theta_x = 0, \pi$. Thus only a Z_2 subgroup of the original $U(1)$ survives when we demand gauge invariance for the states having ± 2 charges in addition to the zero charged ones. (Note that the total charge is still zero, we are only referring to the local charges).

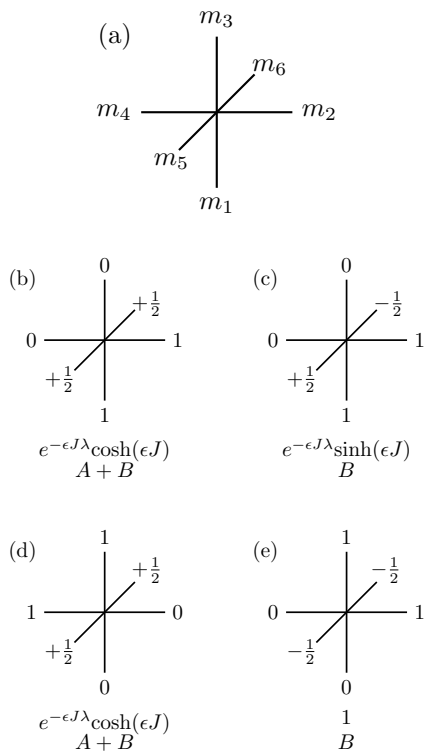


Figure 7. The layout of the height variables and the cluster rules. (a) m_1, m_2, m_3, m_4 lie on a timeslice t , m_5 is on timeslice $t - 1$, and m_6 on timeslice $t + 1$. (b) and (c) Out-of-plane breakups: when there is a reference configuration, one can connect m_5 and m_6 with a certain probability only if they are the same (A -breakup). The B -breakup corresponds to the case when $m_5 \neq m_6$ and they cannot be connected. (d) and (e) In-plane breakups: If $m_5 \neq m_6$, m_1, m_2, m_3, m_4 are in a reference configuration and must be connected, while for $m_5 = m_6$ the connection of m_1, m_2, m_3, m_4 is done with only a certain probability.

Dualization, quantum Monte Carlo algorithm, and order parameters

Construction of efficient quantum Monte Carlo algorithms for (lattice) gauge theories is a particularly difficult challenge due to the constraints that need to be satisfied. Stochastic local updates typically get rejected when they cannot satisfy the constraints, while global updates satisfying detailed balance are non-trivial to construct. Our model, being a lattice gauge theory is no exception. However, recently it has become possible to exploit dualization techniques in order to rewrite the problem in terms of different variables which partially solve the gauge constraints. The $U(1)$ theory in $(2 + 1)$ -d can be dualized into a $(2 + 1)$ -d quantum height model, for which efficient cluster algorithms can be constructed. In particular, rewriting the gauge theory in terms of the height variables completely eliminates the odd charges $Q_x = \pm 1$ from the theory written in terms of the height

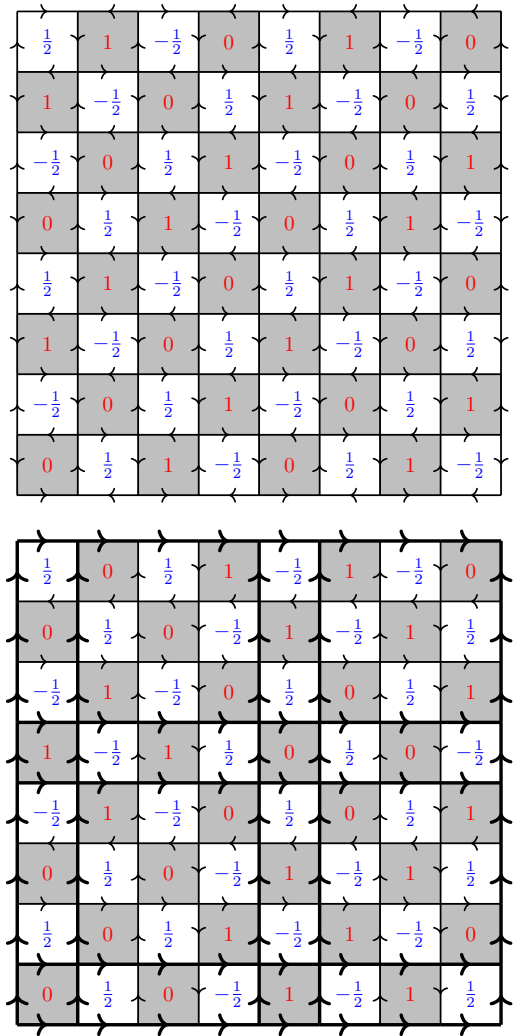


Figure 8. (top) A sample configuration on the $L = 8$ lattice with the largest magnetization for both M_A and M_B , which corresponds to all flippable plaquettes. Both the flux and the height configurations are shown. For this configuration, $M_A = -16$ and $M_B = 16$. (bottom) A different configuration for the $L = 8$ lattice with winding numbers $W_x = W_y = 2$, showing both the height and the flux configurations, for which $M_A = M_B = 0$. The links carrying the winding strings, both in the horizontal and vertical directions, are shown in bold.

variables. The resulting theory only allows $Q_x = 0, \pm 2$, which explains the algorithmic ease of incorporating the ± 2 charges. However, as was done in [30], it is easy to impose a further constraint in the cluster algorithm to project out the ± 2 charges while studying the pure gauge theory. We provide an outline of the procedure below, for further details please see [32].

Equation (1) and Equation (2) display the Hamiltonian and the partition function of our model, respectively. To proceed further, we construct the transfer matrix $\mathbb{T} = e^{-\epsilon H}$, by discretizing the temporal direction into L_T time slices ($\beta = \epsilon L_T$). Moreover, noting that

each link participates in two plaquette interactions, it is natural to divide the lattice into even (A) and odd (B) sublattices, which is the well-known Trotter decomposition. All the plaquettes in sublattice A (or sublattice B) can be considered to be interacting simultaneously. Figure 6 shows the division into two sublattices A and B (shaded and unshaded) respectively. The Hamiltonian and partition function can now be written as,

$$H = H_A + H_B \quad \text{and} \quad Z = \text{Tr} \left[\mathbb{T}_A^{L_T} \mathbb{T}_B^{L_T} P_G \right] \quad (7)$$

where $\mathbb{T}_{A(B)} = \exp[-\epsilon H_{A(B)}]$ and we have neglected $O(\epsilon^2)$ terms. P_G is the projection operator enforcing the Gauss law: $P_G = \prod_x \{6\delta(G_x) + \delta(G_x - 2) + \delta(G_x + 2)\}^{\frac{1}{8}}$ when we need to include the charge ± 2 , or $P_G = \prod_x \delta(G_x)$, for the case without the charges. We can read off the weights for the various configurations from the single plaquette transfer matrix operator:

$$\begin{aligned} \mathbb{T}_\square = & 1 + (U_\square + U_\square^\dagger) e^{-\epsilon \lambda J} \sinh(\epsilon J) \\ & + (U_\square + U_\square^\dagger)^2 [e^{-\epsilon \lambda J} \cosh(\epsilon J) - 1] \end{aligned} \quad (8)$$

The non flippable plaquettes (fourteen of them) have unit weights. The two flippable plaquettes give diagonal contribution of $e^{-\epsilon \lambda J} \cosh(\epsilon J)$. A configuration where a plaquette is flipped has a weight $e^{-\epsilon \lambda J} \sinh(\epsilon J)$ (the off-diagonal elements).

On dualization, the model is reformulated in terms of quantum height variables, which live in the centres of the plaquettes (the dual lattice sites). Thus, if a site is labelled as $x = (x_1, x_2)$, the dual sites (where the dual heights are located) are at $\tilde{x} = (x_1 + \frac{1}{2}, x_2 + \frac{1}{2})$. Moreover, the height variables on different sublattices are distinct: $h_{\tilde{x}}^A = 0, 1$ for even (A) sublattice and $h_{\tilde{x}}^B = \pm \frac{1}{2}$ for odd (B) sublattice. The divergence of the height variables are the electric flux variables,

$$E_{x, \hat{i}} = \left[h_{\tilde{x}}^X - h_{\tilde{x} + \hat{i} - \bar{1} - \bar{2}}^{X'} \right] \text{mod} 2 = \pm \frac{1}{2}; \quad X, X' \in \{A, B\} \quad (9)$$

An example of the flux to height mapping is shown in Figure 6 (left). We note that the above relation remains unchanged when both the height variables are flipped, and thus there are two distinct height configurations which map to a single flux configuration. Moreover, it is easy to check by constructing the height variables in the presence of charges $Q_x = \pm 1$ that the height assignment does not work out, while $Q_x = \pm 2$ does not present a problem. In other words, the dualization using the height variables projects out the $Q_x = \pm 1$.

The cluster algorithm works by building clusters in a single sublattice at a time. Bonds between the variables in a sublattice (say A) are put depending on the value of the height variables in the other sublattice (therefore B), which we now discuss. In Figure 7 (a), the general layout of height variables across time slices is shown: m_1, m_2, m_3 and m_4 lie in time slice t , m_5 lies in time slice $t - 1$ and

m_6 lies in time slice $t + 1$. We shall consider two different breakups, the out-of-plane breakups (whether to bond m_5 and m_6) and in-plane breakups (whether to bond m_1, m_2, m_3 and m_4). If we can bond heights, we call it a A -breakup; otherwise it is a B -breakup.

• Out-of-plane breakups:

- If (m_1, m_2, m_3, m_4) are not in reference configuration, m_5 must be equal to m_6 , and we must bond (m_5, m_6) to forbid disallowed configurations.
- If (m_1, m_2, m_3, m_4) are in reference configuration, either $m_5 \neq m_6$ (weight is $e^{-\epsilon \lambda J} \sinh(\epsilon J)$) or $m_5 = m_6$ (weight is $e^{-\epsilon \lambda J} \cosh(\epsilon J)$). If $m_5 \neq m_6$, have case B (see Figure 7 (c)). If $m_5 = m_6$, both A and B can happen (see Figure 7(b)). To satisfy detailed balance, we have, $P_B = B/(A+B) = \tanh(\epsilon J)$ and $P_A = 1 - P_B = \frac{e^{-\epsilon J}}{\cosh(\epsilon J)}$.

• In-plane breakups:

- If $m_5 \neq m_6$, (m_1, m_2, m_3, m_4) are in a reference configuration and we must bind them together to avoid disallowed configuration.
- If $m_5 = m_6$, either (m_1, m_2, m_3, m_4) are in reference configuration (with weight $e^{-\epsilon \lambda J} \cosh(\epsilon J)$) or they are not (weight is 1). If (m_1, m_2, m_3, m_4) form a reference configuration, both A and B can be applied, else, we are in case B (see Figure 7). Solving the detailed balance equation we get, $P_B = B/(A+B) = \frac{e^{\epsilon \lambda J}}{\cosh(\epsilon J)}$ and $P_A = 1 - \frac{e^{\epsilon \lambda J}}{\cosh(\epsilon J)}$.

The cluster building process proceeds as is usual in a spin model. It is possible to consider the single cluster Wolff algorithm, or the multi-cluster Swendsen-Wang variant. For our case, we have implemented both the algorithm and checked that the answers match.

Another important point is the construction of order parameters, M_A and M_B , which are constructed as $M_X = \frac{1}{L_T} \sum_{\tilde{x}} \eta_{\tilde{x}}^X h_{\tilde{x}}^X$, where $X = A, B$ and \tilde{x} denote the dual sites (centres of the plaquettes of the original space-time lattice). The phases η^X , which need to be multiplied with the height variables h^X to get the magnetization, are displayed in Figure 6 (right) for $L = 4$, but for any other lattice (with a multiple of 4), they can be easily tiled. We note that this order parameter is sensitive to the different confined phases: $C1$ and $C2$. While $C1$ has ordering on both sublattices (and hence have maximum values of both M_A and M_B), $C2$ has order on only one sublattice (so either M_A or M_B is maximum and the other is zero). An example of the $C1$ phase is shown for the $L = 8$ in Figure 8 (top) with both the height and the flux configurations, for which one has $M_A = -16$ and

$M_B = 16$. Interestingly, these order parameters also signal deconfinement by *both* going to zero simultaneously, when the lattice volume has many (extensive) winding strings. An example of a state with winding strings is shown in Figure 8 (bottom), for which $M_A = M_B = 0$.

Methods: Exact diagonalization and cluster QMC

For our model in two spatial dimensions (L_X, L_Y) and spin- $\frac{1}{2}$ degrees of freedom per link, there are $2^{2L_X L_Y}$ possible configurations, while working in the electric flux basis. Imposing the Gauss law constraint (which is easy in the flux basis) greatly reduces the number of allowed basis states in the Hilbert space. For example, a (4,4) lattice with only zero-charges has 2970 basis states, while the same lattice allowing for additional ± 2 -charges has 131072 basis states.

A pragmatic way to proceed is to divide the Hilbert space into various winding number sectors (W_x, W_y). Since these sectors do not mix up among themselves, we can independently work in each individual sector, thus effectively reducing the Hilbert space dimension. In the presence of only $Q = 0$ the individual winding numbers along x or y direction are all the same irrespective of where they are summed. Now, if we allow $Q = \pm 2$ along with $Q = 0$, the individual winding numbers along any direction can, in principle, be different; so we should label these sectors as $(\{W_{x,1}, W_{x,2}, \dots, W_{x,L_Y}\}, \{W_{y,1}, W_{y,2}, \dots, W_{y,L_X}\})$. Interestingly, all the winding numbers along a direction, are either all even or all odd. Thus, there are four sectors: (even, even), (even, odd), (odd, even) and (odd, odd). For a (4,4) lattice, the winding numbers can take values 0, ± 1 and ± 2 . So there are $3^4 \times 3^4$ sub-sectors within (even, even) sector, $3^4 \times 2^4$ sub-sectors within (even, odd) or (odd, even) sector and $2^4 \times 2^4$ sub-sectors within (odd, odd) sector. Thus, the Hilbert space in a given winding sector is further divided into many small sub-sectors which do not mix among themselves, facilitating ED significantly. For a (4,4) lattice, in the presence of only zero charges we need to diagonalize the largest sector (0,0) which has 990 basis states, whereas, in the addition of ± 2 charges we need to diagonalize the largest sector $(\{0, 0, 0, 0\}, \{0, 0, 0, 0\})$ with 3464 basis states.

Our QMC cluster algorithm can simulate different winding number sectors, but the height representation constrains the winding sectors that can be simulated at a time. For example, using periodic boundary conditions, only even winding sectors can be simulated, while for odd winding sectors one would need anti-periodic boundary conditions. While this is irrelevant for infinite volume in the spatial directions, it is important in the shorter temporal directions to have periodic boundary conditions on the height variables. Periodic boundary conditions on the flux variables translate to both *periodic* and *anti-*

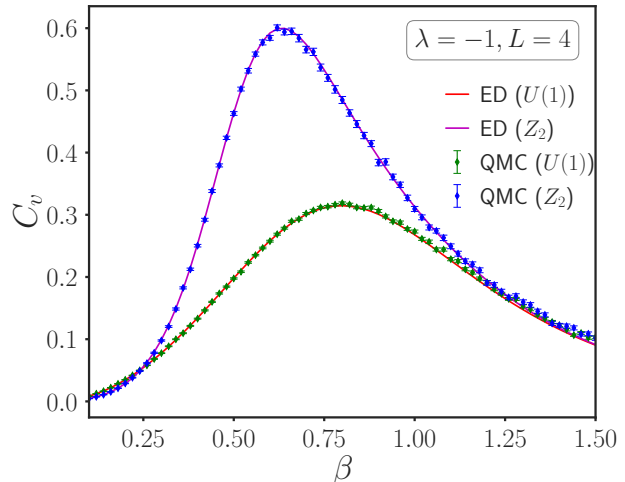


Figure 9. Comparison of ED and QMC.

periodic boundary conditions on the height variables in time. However, the latter gives rise to an interface, which would become energetically unfavourable when one approaches the thermodynamic limit. Thus, it is completely natural to use the QMC on the height variables and restrict oneself to the even winding sectors.

In Figure 9 we have plotted specific heat, $C_v = \beta^2(\langle E^2 \rangle - \langle E \rangle^2)$ versus β , obtained using QMC and ED for both absence and presence of $Q = \pm 2$. Here $\langle E \rangle = -\frac{\partial \ln Z}{\partial \beta} = -\frac{1}{L_T} \frac{\partial \ln Z}{\partial \epsilon}$ is average energy and $\langle E^2 \rangle = \frac{1}{Z} \frac{\partial^2 Z}{\partial \beta^2} = \frac{1}{Z L_T^2} \frac{\partial^2 Z}{\partial \epsilon^2}$ is the average of energy squared, where the partition function is $Z = \sum_{\text{config.}} \prod_{\square} W_{\square}(\epsilon J, \epsilon \lambda)$. W_{\square} is the weight associated with a certain 6-height-variables interaction. W_{\square} can take values $W_{\square}^1 = e^{-\epsilon J \lambda} \sinh(\epsilon J)$ for a flipped plaquette, $W_{\square}^2 = e^{-\epsilon J \lambda} \cosh(\epsilon J)$ for an unchanged flippable plaquette and $W_{\square}^3 = 1$ otherwise. After simplification, $\langle E \rangle = -\frac{1}{L_T} \langle \sum_{\square} \frac{\partial \ln W_{\square}}{\partial \epsilon} \rangle$ and $\langle E^2 \rangle$ reads as $\frac{1}{L_T^2} \left(\langle \sum_{\square} \frac{\partial^2 \ln W_{\square}}{\partial \epsilon^2} \rangle + \langle \sum_{\square} \left(\frac{\partial \ln W_{\square}}{\partial \epsilon} \right)^2 \rangle \right)$. To compute $\langle E \rangle$ and $\langle E^2 \rangle$ using QMC, we need to go through all 6-height-variables interactions and check the corresponding weights associated with them and add the appropriate factors in accordance with the simplified forms of $\langle E \rangle$ and $\langle E^2 \rangle$.

We note the nice agreement of results between QMC and ED in Figure 9, which indicates the efficiency of the cluster algorithm we have used.

Variation of local charge density with temperature

While the $U(1)$ QLM has $\langle Q^2 \rangle = 0$ (normalized with the spatial volume) at all T and λ by definition, this is not the case for the LGT defined by the partition function in

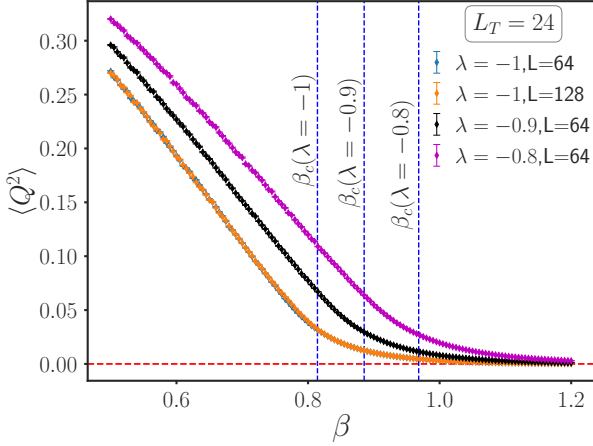


Figure 10. The $\langle Q^2 \rangle$ operator for different values of λ for a range of β on our finest lattice, $L_T = 24$. The vertical dotted line shows the location of critical temperature for the different λ values.

Equation (2). For example, it is easy to see that $\langle Q^2 \rangle \rightarrow 1$ as $T \rightarrow \infty$ from Equation (2). On the other hand, the mass gap of $Q = \pm 2$ charges scale as $O(|\lambda|)$ from Equation (1) for negative values of λ which implies that $\langle Q^2 \rangle \sim \exp(-a|\lambda|/T)$, where a is an $O(1)$ number, as $T \rightarrow 0$.

In Fig. 10, we show the variation of $\langle Q^2 \rangle$ as a function of β from the QMC data for the $U(1)$ QLM with $Q = \pm 2$ (Equation (2)) for $\lambda = -1.0, -0.9, -0.8$ respectively using $L_T = 24$. At low T and also in the neighborhood of $T_c = 1/\beta_c$, $\langle Q^2 \rangle$ follows an activated behavior of $\exp(-a|\lambda|/T)$ for all the three values of λ . Interestingly, even though $\langle Q^2 \rangle \approx 0.03$ in the vicinity of β_c and thus the $Q = \pm 2$ charges can be considered to be dilute at the deconfinement transition, this thermal population is sufficient to completely change the critical behavior compared to the case where $\langle Q^2 \rangle$ is strictly zero. We thus conjecture that these charged degrees of freedom ($Q = \pm 2$) generate a marginal operator and hence, weak universality in this LGT.